Energy-maximising experimental control synthesis via impedance-matching for a multi degree-of-freedom wave energy converter

Available online at www.sciencedirect.com

ScienceDirect

IFAC Papers Online CONFERENCE PAPER ARCHIVE

IFAC PapersOnLine 55-31 (2022) 345–350

Energy-maximising experimental control synthesis via impedance-matching for a multi degree-of-freedom wave energy converter ⋆

Nicolás Faedo [*,1] **Edoardo Pasta** [*] **Fabio Carapellese** [*] **Vincenzo Orlando** [**] **Domenica Pizzirusso** [***] **Dario Basile** [****] **Sergej A. Sirigu** [*]

[*] *Marine Offshore Renewable Energy Lab., Dept. of Mechanical and Aerospace Engineering, Politecnico di Torino, Italy.*
[**] *Wave for Energy S.R.L.*
[***] *EniProgetti*
[****] *Eni, S. p. A.*

Abstract: We present, in this paper, an experimental framework for design and synthesis of impedance-matching-based (IM) controllers capable of maximising energy extraction in inherently multi degree-of-freedom wave energy converter (WEC) systems, and its subsequent application to the Intertial Sea Wave Energy Converter (ISWEC) device, by incorporating recent advances in IM-based theory. In particular, we consider a 1/20th scale prototype of the ISWEC system, tested as part of a larger experimental campaign conducted within the tank facilities available at Università degli Studi di Napoli Federico II, subject to a variety of wave conditions. We adopt two different control structures to realise an approximation of the IM principle, fully tuned based upon interpolation of a particular (experimentally obtained) non-parametric empirical transfer function estimate, which defines the optimal frequency-domain input-output response for energy-maximising behaviour. Furthermore, a performance comparison between controller tuning based upon traditional linear boundary element method models, and the presented experimental approach, is also offered, showing that the latter can consistently outperform the former in realistic scenarios, for the set of analysed sea-states.

Keywords: Wave energy converters, Optimal control, Impedance-matching

1. INTRODUCTION

The pathway towards achieving commercial viability of wave energy converter (WEC) systems inherently incorporates design and synthesis of tailored control technology, capable of maximising the extraction of the wave resource, hence contributing in lowering the associated levelised cost of energy (Ringwood, 2020). Recent years have seen an increase in the number of potential control strategies proposed to fulfill this purpose, with a specific focus in exhibiting practical viability (*e.g.* well-posed control solutions, real-time performance, constraint handling).

Proposing solutions able to deal with this issue of practical viability becomes significantly more complex when dealing with intrisically multiple degree-of-freedom (DoFs) WEC systems, *i.e.* devices which can naturally move in multiple modes of motion. Furthermore, the vast majority of these inherently multi-DoF devices are also underactuated, which incorporates an additional degree of complexity within the definition of the associated optimal control problem (Korde and Ringwood, 2016). Such is the case of the Inertial Sea Wave Energy Converter (ISWEC), a gyroscope-based floating WEC device originally proposed in (Bracco et al., 2011), which is the main subject of our study. This device, described in detail within Section 2, is allowed to move in eight DoFs, with energy conversion effectively happening in a subset of two DoFs, corresponding with two enclosed gyroscopic systems.

The fundamental principle of impedance-matching (IM) (Thomas, 1976) has inspired a number of sophisticated, yet simple, control strategies for WECs (see *e.g.* García-Violini et al. (2020); Faedo et al. (2020)). In essence, the WEC system is treated as a 'circuit', and the objective becomes that of designing a suitable control 'load' such that maximum energy transfer is achieved from the source (*i.e.* the wave field). In particular, this family of controllers is based upon the idea of providing implementable (causal - often linear time invariant) solutions to the non-causal optimal energy-maximising condition arising from the IM principle, hence having the capability of maximising energy absorption with mild computational requirements, being often intuitive in their design, and hence especially appealing within realistic (real-time) applications (García-Violini et al., 2020).

⋆ Nicolás Faedo has received funding from the European Union's Horizon 2020 research and innovation programme under the Marie Sklodowska-Curie grant agreement No 101024372.
[1] Corresponding author - e-mail: *nicolas.faedo@polito.it.*

10.1016/j.ifacol.2022.10.453

Motivated by the suitability of this family of controllers, this paper presents an experimental framework for synthesis of IM-based controllers for inherently multi-DoF systems, and its subsequent application to the ISWEC system, by incorporating recent advances in IM theory for multiple degree-of-freedom WEC systems (Faedo et al., 2022). In particular, we consider a 1/20th scale prototype of the ISWEC device, tested as part of a larger experimental campaign conducted within the tank facilities available at Università degli Studi di Napoli Federico II, subject to a variety of wave conditions. We adopt two different control structures to realise an approximation of the IM principle, namely coupled proportional, and coupled proportional-integral, controllers, fully tuned based upon interpolation of a particular non-parametric empirical transfer function estimate (ETFE), which defines the optimal frequency-domain input-output response for energy-maximising behaviour. We show that the corresponding optimal ETFE can be fully characterised in terms of *measurable variables*, and can be computed experimentally via classical system identification procedures. We note that, to the best of our knowledge, this paper presents the first experimental application of the IM principle for underactuated multi-DoF systems (as presented in Faedo et al. (2022)) for WEC control design purposes, showing the feasibility behind such an approach for the computation of practically viable WEC controllers, being hence ideal for realistic scenarios. Furthermore, a performance comparison between controller tuning based upon traditional linear boundary element method (BEM) models, and the presented experimental approach, is also included, showing that the latter can consistently outperform the former in realistic scenarios.

The reminder of this paper is organised as follows. Section 1.1 introduces the notation used throughout our study, while Section 2 presents the ISWEC prototype and the corresponding experimental setup. Section 3 discusses the derivation of the IM principle for the ISWEC system, and its subsequent use for control design and synthesis. Section 4 presents the experimental results obtained as part of this study, including system identification, synthesis of causal controllers, performance assessment. Finally, Section 5 elucidates the main conclusions of this study, together with a set of further directions to explore in the near future.

1.1 Notation

$\mathbb{R}^+$ and $\mathbb{C}^0$ are used to indicate the set of non-negative real numbers, and the set of complex numbers with zero real-part, respectively. $\mathbb{N}_p$ is used to indicate the set of positive natural numbers up to p, *i.e.* $\mathbb{N}_p = \{1, 2, \dots, p\}$, while $\mathbb{I}_p$ indicates the identity element of the space $\mathbb{C}^{p\times p}$. The notation $\Re(s)$ and $\Im(s)$ is used to indicate the real- and imaginary-parts of $s \in \mathbb{C}$, respectively. Given a matrix $A \in \mathbb{C}^{n\times n}$, the notation $\lambda(A) \subset \mathbb{C}$ indicates its set of eigenvalues. The Laplace transform of a function f, provided it exists, is denoted as $F(s)$, $s \in \mathbb{C}$. The Hermitian operation is denoted by $F(\jmath\omega)^\star$, with $\omega \in \mathbb{R}$, while, with some abuse of notation, the Hermitian-inverse composition is denoted as $(F^\star)^{-1} = F^{-\star}$. Finally, the notation $\mathcal{RH}_\infty$ is used for the set of real rational proper and stable functions $G : s \mapsto G(s)$, $s \in \mathbb{C}$, while $\mathcal{RH}_2$ is considered for the set of *strictly* proper and stable functions in $\mathbb{C}$.

2. DEVICE AND EXPERIMENTAL SETTING

The ISWEC system is a wave energy conversion device featuring a flywheel system, exploiting the associated gyroscopic effect to convert kinetic energy available via pitch motion of its hull. This characteristic makes it a reactive inertial-based WEC, and a pitch-resonant device, with its hull being specifically designed to enable and enhance pitch motion. As such, the associated mooring system is tailored both to ensure station-keeping, and adapt the direction of the hull in line with the principal direction of the incident wave, allowing the device to 'self-align' with the incoming wave field.

The system features two gyroscopic units, which are constituted by spinning flywheels, housed inside the WEC hull. The adoption of an even number of gyroscopes allows effective pairing of both units, each one having an opposite flywheel orientation and speed with respect to the other. This configuration is considered to minimise the exerted roll gyroscopic torque. The dynamic coupling between pitch motion and spinning flywheel induces a precession phenomenon, whose mechanical energy is converted through the incorporated power take-off (PTO) system. In the case of the prototype considered within this study, the PTO system is composed of a pair of permanent magnet synchronous motors, connected to each corresponding gyroscope frame by means of independent gearboxes. The specific 1/20th scale ISWEC prototype, considered in this paper, is shown in Figure 1.

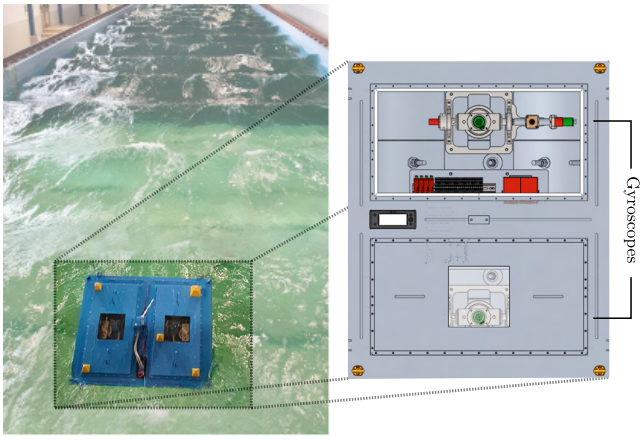

Fig. 1. ISWEC 1/20th scale prototype in the wave basin.

With respect to the experimental setting, the device is sitting in a wave basin with a width of 9 [m], and length of 147 [m], while the water depth can be adjusted up to 4.2 [m], by virtue of a movable floor. Wave generation is performed via an associated wavemaker, specifically through 24 individually controlled hinged flap paddles, incorporating wave absorption capabilities. The ISWEC prototype is moored to a virtual seabed, built specifically for this experimental campaign, using twenty fiberglass panels connected by steel junctions, connected through steel flanges and positioned in two lines of ten panels each. An inertial measurement unit (IMU) MTi 100 (Xsens) system is used to measure the device motion in all six hydrodynamic DoF, and the effective motion of each of the two gyroscopic DoFs, which is subsequently used to perform system identification routines in Section 4.

3. IM-BASED CONTROL DESIGN AND SYNTHESIS

From now on, we assume the full WEC system, presented in Section 2, can be reasonably described, from an input-output perspective, in terms of a *representative* [2] linear operator $G^0 : \mathbb{C}^0 \to \mathbb{C}^{8\times 8}$, $s \mapsto G^0(s) \in \mathcal{RH}_2$, with each of the eight DoFs defined (and ordered) as in Table 1. The first six DoFs, *i.e.* the so-called hydrodynamic modes, are affected by a set of external (uncontrollable) inputs $\mathscr{F}_{\rm e} = \{f_{{\rm e}_i}\}_{i=1}^6$ referred to as *wave excitation forces*, descrbing the force exerted by the incoming wave field on the WEC system. The last two DoFs, *i.e.* seven and eight, correspond with each gyroscope axis (see Section 2), and are affected by a user-supplied PTO (controllable) force, defined via the set $\mathscr{U} = \{u\}_{i=1}^2$. Let $\mathscr{Y} = \{y\}_{i=1}^8$ denote the set of outputs (set to be velocities) associated with each DoF, according to the ordering provided in Table 1, so that the map $G^0_{ij} : \mathbb{C}^0 \to \mathbb{C}$ represents the transfer function from the input acting on the i-th DoF, to the output corresponding with the j-th DoF, for $\{i, j\} \subset \mathbb{N}_8$.

Table 1. DoFs characterising the ISWEC.

DoF #	Description	Input	Output
1	Surge	$f_{\rm e_1}$	y_1
2	Sway	$f_{\rm e_2}$	y_2
3	Heave	$f_{\rm e_3}$	y_3
4	Roll	$f_{\rm e_4}$	y_4
5	Pitch	$f_{\rm e_5}$	y_5
6	Yaw	$f_{\rm e_6}$	y_6
7	Gyroscope motion 1	u_1	y_7
8	Gyroscope motion 2	u_2	y_8

The set of PTO forces $\mathscr{U}$ is to be designed such that the following map (control objective)

$$(u_1, u_2) \mapsto \int_{\mathbb{R}^+} (y_7 u_1 + y_8 u_2)\, {\rm d}t, \tag{1}$$

is maximised, *i.e.* such that maximum energy absorption from the incoming wave field is achieved by the two available gyroscope systems. As anticipated in Section 1, throughout this paper, we adopt a frequency-domain approach to solving the optimal control problem associated with the maximisation of (1), via recent advances in so-called IM principle. The study presented in (Faedo et al., 2022) presents a general energy-maximising framework for multi-DoF underactuated WEC systems, such as the ISWEC system, providing a set of optimality conditions which can be used to synthesise (u_1, u_2) so as to achieve maximum energy absorption from the incoming wave field. We discuss the application of such a principle, for the ISWEC system, in the following paragraphs.

Let $y = [y_1 \dots y_8]^\mathsf{T}$, $f_{\rm e} = [f_{\rm e_1} \dots f_{\rm e_6}]^\mathsf{T}$, and $u = [u_1\, u_2]^\mathsf{T}$, be the output, excitation force, and control force vectors, respectively, and hence the action of the map G^0 can be written, in the frequency-domain, as

$$Y(\jmath\omega) = G^0(\jmath\omega) \begin{bmatrix} F_{\rm e}(\jmath\omega) \\ U(\jmath\omega) \end{bmatrix}. \tag{2}$$

[2] The term 'representative' refers here to linear models which can cater for specific operating conditions, as opposed to standard linear operators derived via Jacobian linearisation about the zero equilibrium (see *e.g.* Davidson et al. (2015))

Given the control objective in (1), we are particularly interested in the frequency-domain behaviour of the map $(u_1, u_2) \mapsto (y_1, y_2)$, which can be expressed via (2) as [3]

$$Y_u = \begin{bmatrix} G^0_{\bar{u}} & G^0_u \end{bmatrix} \begin{bmatrix} F_{\rm e} \\ U \end{bmatrix}, \tag{3}$$

with

$$Y_u = \begin{bmatrix} Y_7 \\ Y_8 \end{bmatrix}, G^0_u = \begin{bmatrix} G^0_{77} & G^0_{78} \\ G^0_{87} & G^0_{88} \end{bmatrix}, G^0_{\bar{u}} = \begin{bmatrix} G^0_{11} & \dots & G^0_{16} \\ \vdots & \ddots & \vdots \\ G^0_{16} & \dots & G^0_{66} \end{bmatrix}, \tag{4}$$

where Y_u denotes the vector of controlled outputs, and the mappings $G^0_{\bar{u}}$ and G^0_u describe the dynamics associated to controlled and uncontrolled DoFs, respectively.

Remark 1. Note that $G^0_{\bar{u}}$ explicitly defines the 'contribution' of the wave excitation forces acting on the first six hydrodynamic modes of motion, which is, ultimately, what (externally) drives both gyroscope systems (see Section 2).

Equation (3) can be expressed equivalently as

$$Y_u = G^0_u \left[\tilde{F}_{\rm e} - U \right], \tag{5}$$

where the map $\tilde{F}_{\rm e}$, defined as

$$\tilde{F}_{\rm e} = {G^0_u}^{-1} G^0_{\bar{u}} F_{\rm e}, \tag{6}$$

denotes the so-called *total wave excitation force* (see Faedo et al. (2022)) acting on the controlled modes of motion, *i.e.* the gyroscopic degrees-of-freedom. Note that $0 \notin \lambda(G^0_u(\jmath\omega))$, for every admissible ω, given the physics associated with the WEC process.

From equation (5), we can define the so-called intrinsic impedance of the gyroscopic modes of motion simply as

$$I^0 = {G^0_u}^{-1}, \tag{7}$$

so that the WEC system (3) can be seen as a 'circuit', characterised by an internal load I^0, excited by the external source $\tilde{F}_{\rm e}$. A direct application of the impedance-matching principle allows for the computation of the (frequency-domain) optimal energy-maximising control input (force), via (7), as

$$U = -I_u Y_u = -I^{0^\star} Y_u = -{G^0_u}^{-\star} Y_u, \tag{8}$$

where I_u denotes the control 'load', and hence (8) effectively describes a feedback control structure. The optimal closed-loop response, characterising the map $T^{\rm opt} : \tilde{F}_{\rm e} \mapsto Y_u$ under controlled conditions, can be written as

$$T^{\rm opt} = \left(\mathbb{I}_2 + G^0_u I_u \right)^{-1} G^0_u. \tag{9}$$

Remark 2. Though one can be tempted to use the analytic continuation of $I_u = I^{0^\star}$ in the Laplace-domain to effectively implement (8), the resulting transfer function is inherently non-causal due to the nature of the corresponding analytic continuation of the Hermitian operator (see *e.g.* Fuhrmann (1989)). Nonetheless, one can effectively approximate the control condition (8) via stable and causal control structures, as discussed in the following.

In particular, in the light of Remark 2, we consider the following two different feedback control structures for the experimental campaign performed on the ISWEC system, presented herein within Section 4:

[3] As of this moment, we omit the dependence on $\jmath\omega$ when clear from the context.

$$K^{\mathrm{P}}(s) = \begin{bmatrix} \theta_{11}^{\mathrm{P}} & \theta_{12}^{\mathrm{P}} \\ \theta_{21}^{\mathrm{P}} & \theta_{22}^{\mathrm{P}} \end{bmatrix}, \\ K^{\mathrm{PI}}(s) = \begin{bmatrix} \theta_{11}^{\mathrm{PI}} + \frac{1}{s}\kappa_{11}^{\mathrm{PI}} & \theta_{12}^{\mathrm{PI}} + \frac{1}{s}\kappa_{12}^{\mathrm{PI}} \\ \theta_{21}^{\mathrm{PI}} + \frac{1}{s}\kappa_{21}^{\mathrm{PI}} & \theta_{22}^{\mathrm{PI}} + \frac{1}{s}\kappa_{22}^{\mathrm{PI}} \end{bmatrix}, \tag{10}$$

where $\{K^{\mathrm{P}}(s), K^{\mathrm{PI}}(s)\} \subset \mathcal{RH}_\infty$ correspond with (coupled) MIMO proportional (P), and proportional-integral (PI) control structures, respectively. Following (Faedo et al., 2022), the sets of coefficients $\Theta^{\mathrm{P}} = \{\theta_{ij}^{\mathrm{P}}\}_{(i,j)\in\mathbb{N}_2} \subset \mathbb{R}^+$ and $\Theta^{\mathrm{PI}} = \{\theta_{ij}^{\mathrm{PI}}\}_{(i,j)\in\mathbb{N}_2} \cup \{\kappa_{ij}^{\mathrm{PI}}\}_{(i,j)\in\mathbb{N}_2} \subset \mathbb{R}$, are defined such that the following set of interpolation conditions

$$K^{\mathrm{P}}(\jmath\omega_I) = |I_u(\jmath\omega_I)|, \quad K^{\mathrm{PI}}(\jmath\omega_I) = I_u(\jmath\omega_I), \tag{11}$$

holds, where $\omega_I \in \mathbb{R}^+$ denotes a suitably chosen interpolation frequency. The specific selection of ω_I is discussed in detail throughout Section 4.

Remark 3. Synthesis of K^P and K^{PI}, and any other potential implementable structure, only depends upon the dynamics of the controlled DoFs, *i.e.* G_u^0 in (3). In other words, the determination of the frequency-domain behaviour of G_u^0, *i.e.* the map $(u_1, u_2) \mapsto (y_7, y_8)$, is sufficient to compute the optimal condition (8), subsequently used to synthesise (10). Note that both input channels (u_1 and u_2), and the corresponding set of outputs (y_7 and y_8), are accessible and measurable, respectively, so that $G_u^0(\jmath\omega)$ can be computed via standard system identification procedures, as effectively performed in Section 4.

4. EXPERIMENTAL RESULTS

This section presents a set of experimental results obtained within a prototype-testing campaing conducted at the wave tank located in the facilities of Università degli Studi di Napoli Federico II during the period October-November 2021. In particular, we present the experimental determination of the optimal control impedance I_u in (8) for the ISWEC prototype described in Section 2, and the subsequent tuning and synthesis of the (implementable) control structures defined in (11). Before providing a description of such control tuning procedure, we make explicit the set of operating conditions considered, which are subsequently used for performance evaluation.

We consider three different sea-states (SS), each described stochastically in terms of a corresponding JONSWAP-type (Ochi, 1998) spectral density function (SDF), with parameters as described in Table 2, where H_s, T_e and κ denote significant wave height, energetic period, and peak-enhacement factor, respectively. Each SS realisation, generated within the tank via the available mechanical wave-maker system, consists of approximately 10 minutes ($\approx$ 600 typical peak periods per sea condition), always guaranteeing statistically consistent performance results. Experimental and theoretical SDFs are shown, for each SS, in Figure 2.

Table 2. Considered sea-states (SS).

SS #	Parameters		
	H_s	T_e	γ
1	7.87 [cm]	1.23 [s]	3.3
2	10.99 [cm]	1.45 [s]	3.3
3	6.5 [cm]	1.18 [s]	3.3

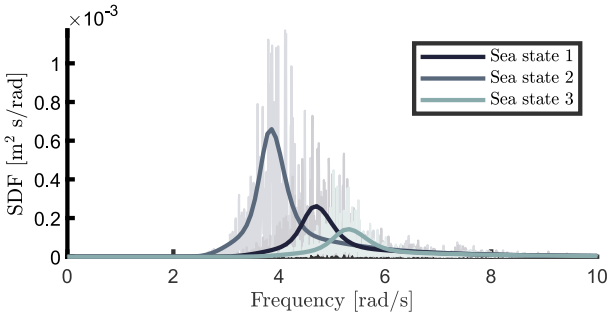

Fig. 2. Experimental and theoretical SDFs considered.

4.1 Experimental $\{G_u^0, I_u\}$ and synthesis of $\{K^P, K^{PI}\}$

We now briefly describe the procedure for the computation of the impedance-matching-based control load I_u in (8), via experimental determination of the map G_u^0 in (4). To achieve such an objective, the device is placed in the tank in absence of waves, *i.e.* in calm water, so that the total wave excitation force in (5) is $\tilde{f}_{\mathrm{e}} = 0$. A set of up-chirp signals $\{u_i^{\mathrm{ID}}\}$, with different amplitudes and frequency content within a set $\mathscr{W}$, covering the range of operating conditions of the WEC system according to the SS listed in Table 2, is considered to excite the system via the input channels corresponding with each gyroscope. In particular, the set $\mathscr{W}$ has been chosen as $\mathscr{W} = [1, 30]$ [rad/s], which fully covers the frequency range containing significant wave energy (see Figure 2). The selected up-chirp signals u_i^{ID} are injected into gyroscopes 1 and 2, both independently, and in a combinated fashion, as per standard MIMO identification procedures (see *e.g.* Ljung (1999)). A subsequent set of outputs, *i.e.* gyroscope velocities y_i^{ID}, is consequently measured, for each corresponding input experiment. With the information of each corresponding input-output pair, the so-called average empirical transfer function estimate (aETFE) $\tilde{G}(\jmath\omega)$ can be constructed (see *e.g.* Ljung (1999)), such that

$$\tilde{G}_u(\jmath\omega) \approx G_u^0(\jmath\omega), \quad \forall\omega \in \mathscr{W}. \tag{12}$$

To provide a first graphical appraisal regarding the determination of the associated aETFE, Figure 3 shows the Bode plot of the $(1,1)$ element of $\tilde{G}_u(\jmath\omega)$ (solid-black line), which provides an experimental characterisation of the map $u_1 \mapsto y_7$. For the sake of completeness, the dotted-grey lines in Figure 3 show magnitude and phase of each individual ETFE, for each considered input-output experiment. Note that, while both within operating and high frequency range, the variability in magnitude and phase for each individual ETFE is rather small (which effectively validates the adopted linearity assumptions), the response for each individual experiment changes rather drastically in the low frequency area. This can be explained, at least partially, by the significant presence of (nonlinear) friction effects in each gyroscope, which, due to the (small) scale of the tested prototype, become almost dominant in low frequency [4]. Finally, a full account of the computed aETFE can be appreciated in Figure 4, which illustrates the singular values (*i.e.* sigma plot) of $\tilde{G}_u(\jmath\omega)$.

Remark 4. Both singular value plots, shown in Figure 4, present slightly different behaviour, even within the oper-

[4] We note that the experimental nonlinear identification of such friction effects, for this same prototype, is subject of ongoing work.

ating frequency range. This indicates that, though theoretically identical, the gyroscopes exhibit slightly different dynamical behaviour, and hence $\tilde{G}_u(\jmath\omega)$ is not symmetric. This is further discussed in Section 4.2.

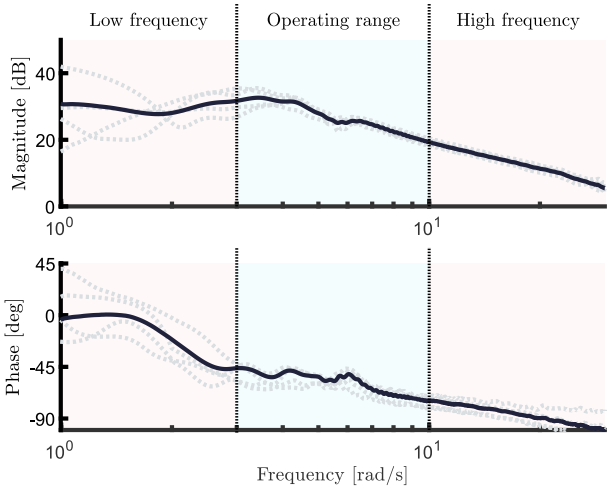

Fig. 3. Bode plot of the $(1,1)$ element of $\tilde{G}_u(\jmath\omega)$ (solid-black line). For the sake of completeness, the dotted-grey lines show individual ETFE behaviour.

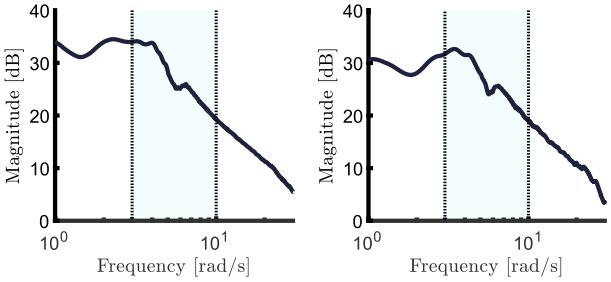

Fig. 4. Sigma plot of $\tilde{G}_u(\jmath\omega)$. The blue area indicates the operating range according to the selected sea-states.

With the computation of the aETFE $\tilde{G}_u(\jmath\omega)$, the associated experimental control impedance $\tilde{I}_u(\jmath\omega) \approx I_u(\jmath\omega)$ for the ISWEC prototype system (as in equation (8)), can be computed in a straightforward fashion, *i.e.*

$$\tilde{I}_u(\jmath\omega) = \begin{bmatrix} \tilde{I}_{u11}(\jmath\omega) & \tilde{I}_{u12}(\jmath\omega) \\ \tilde{I}_{u21}(\jmath\omega) & \tilde{I}_{u22}(\jmath\omega) \end{bmatrix} = (\tilde{G}_u(\jmath\omega))^{-\star}, \qquad (13)$$

for $\omega \in \mathscr{W}$. With equation (13), the experimental determination of the sets of parameters Θ^{P} and Θ^{PI}, defining the control structures in (11) for a given interpolation frequency ω_I, becomes straightforward, *i.e.*

$$\begin{aligned} &\theta^{\mathrm{P}}_{ij} = |\tilde{I}_{u_{ij}}(\jmath\omega_I)|, \\ &\theta^{\mathrm{PI}}_{ij} = \Re(\tilde{I}_{u_{ij}}(\jmath\omega_I)), \quad \kappa^{\mathrm{PI}}_{ij} = -\omega_I \Im(\tilde{I}_{u_{ij}}(\jmath\omega_I)), \end{aligned} \qquad (14)$$

for every $\{i,j\} \in \mathbb{N}_2$. Within this study, the interpolation point ω_I is chosen according to each specific SS considered. In particular, we consider the frequency associated with each corresponding energetic period T_e in Table 2, *i.e.* $\omega_I = 2\pi/T_e$. By way of example, Figure 5 (top) shows the singular values associated with both the empirical optimal controller response $\tilde{I}_u(\jmath\omega)$ (solid-black), and that associated with the causal and stable feedback controller K^{PI} (solid-gray), as in (10), with parameters synthesised as in (14) for an interpolation point (denoted with a green dot) corresponding with SS 1, *i.e.* $\omega_I = 2\pi/5.5$ [rad/s]. In addition, Figure 5 (bottom) shows the sigma plot associated with the closed-loop response (as in equation (9)) for the optimal empirical controller response $\tilde{I}_u(\jmath\omega)$, and that arising from the frequency-response map of K^{PI}.

Remark 5. Though interpolation of the experimental optimal control impedance in a single point might seem somewhat 'limiting' at first sight, we note that the obtained closed-loop frequency-domain behaviour effectively provides a good approximation within the full operating range (in terms of associated singular values), as can be appreciated in Figure 5 (bottom).

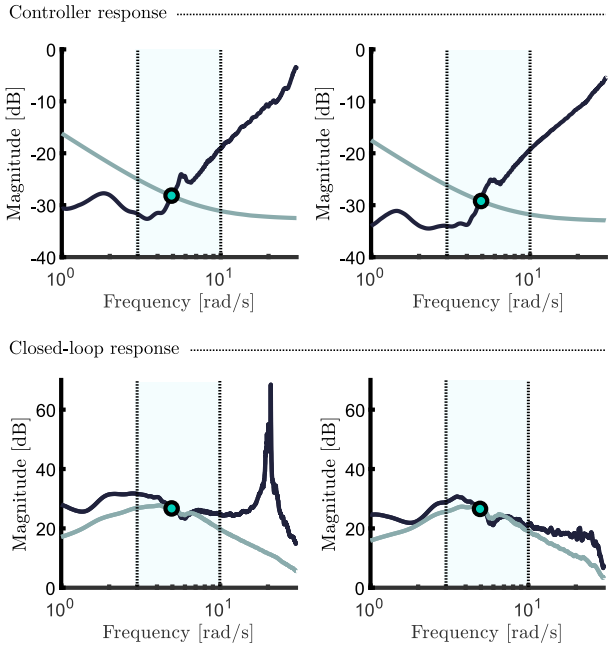

Fig. 5. Top: Sigma plot associated with $\tilde{I}_u(\jmath\omega)$ (solid-black), and $K^{\mathrm{PI}}(\jmath\omega)$ (solid-gray), for $\omega_I = 2\pi/5.5$ [rad/s] (denoted with a green dot). Bottom: Sigma plot for the closed-loop response for $\tilde{I}_u(\jmath\omega)$, and $K^{\mathrm{PI}}(\jmath\omega)$, using the same convention.

4.2 Performance assessment

This section presents a performance assessment of the controllers synthesised in Section 4.1, in terms of effective power absorption. In particular, Figure 6 shows normalised power absorpion for K^{P} (P control - left) and K^{PI} (PI control - right), synthesised based upon the experimentally computed optimal IM response (green), as detailed in Section 4.1, for each specific sea-state. Furhermore, Figure 6 also includes normalised performance for the same control structures posed in (10), but tuned via linear BEM solvers (red), *i.e.* with a G^0_u model computed both by assuming a infinitesimal device motion, and a small-angle approximation for the gyroscope dynamics. For all cases, the normalisation is performed against the maximum energy absorption value obtained, which is achieved by the experimental-based PI control structure K^{PI} in SS 1.

Note that the PI controller is effectively able to enhance the energy-maximising bandwith of the closed-loop WEC system, being capable of increasing energy absorption

consistently for all the considered SS, as opposed to the (more rudimentary) P control, which can only interpolate the magnitude of the associated optimal control condition. Moreover, note that the controllers tuned via experimental determination of the associated aETFE consistently outperform those tuned via BEM-based models, further stressing the non-representative nature of control structures synthesised based upon Jacobian linearisation about the zero-equilibrium of the WEC system (see also the arguments posed in Davidson et al. (2015)), especially in realistic multi-DoF underactuated systems. Finally, and to provide a time-domain appraisal of the gyroscopic behaviour, Figure 7 shows a time-snippet of normalised [5] instantaneous power for both gyroscopes 1 and 2, when the device is subject to SS 2. Note that, consistently with the design procedure, the PI controller intrinsically demands reactive (*i.e.* negative) power flow, required to enforce 'resonance' with the incoming wave field, and hence consequently outperforming the (purely passive) P controller. We further note that, as discussed for the frequency-domain behaviour in Remark 4, the gyroscopes effectively present a different dynamical behaviour, with power peaks taking place at slightly different time instants, and different reactive power flow requirements.

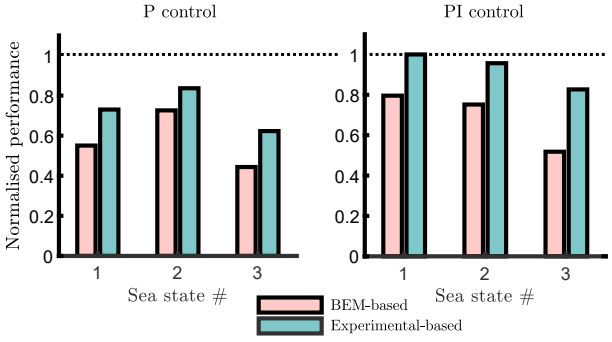

Fig. 6. Normalised power absorpion for P control (left) and PI control (right), tuned experimentally (green) and via BEM-based models (red).

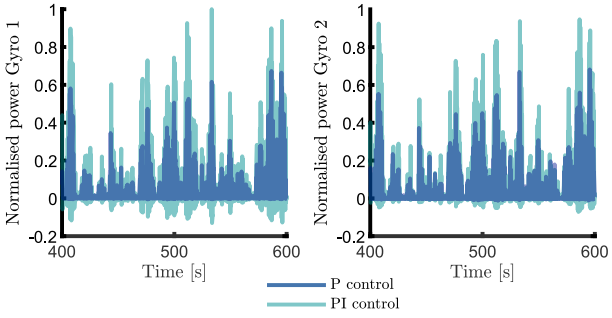

Fig. 7. Time-snippet of normalised instantaneous power for both gyroscopes 1 and 2, for SS 2.

5. CONCLUSIONS AND FUTURE DIRECTIONS

This paper considers the IM principle for multi-DoF underactuated systems presented in (Faedo et al., 2022), for experimental design and synthesis of energy-maximising WEC controllers, with specific application to a prototype of the ISWEC system. We consider two different implementable control structures, fully computed via determination of the aETFE characterising the controlled modes of motion only, which can be performed via standard system identification procedures. This paper represents, to the best of our knowledge, the first experimental application of the multi-DoF IM principle for WEC control design, showing the feasibility of this approach for the computation of practically viable WEC controllers, being hence ideal for realistic scenarios. Future work will consider more sophisticated control structures for the approximation of the IM principle, such as those presented in *e.g.* (García-Violini et al., 2021; Fusco and Ringwood, 2012), aiming at further improving the performance obtained.

[5] Normalised against the maximum peak value achieved by each gyroscope in that specific SS.

REFERENCES

Bracco, G., Giorcelli, E., and Mattiazzo, G. (2011). Iswec: A gyroscopic mechanism for wave power exploitation. *Mechanism and machine theory*, 46(10), 1411–1424.

Davidson, J., Giorgi, S., and Ringwood, J.V. (2015). Linear parametric hydrodynamic models for ocean wave energy converters identified from numerical wave tank experiments. *Ocean Engineering*, 103, 31–39.

Faedo, N., Carapellese, F., Pasta, E., and Mattiazzo, G. (2022). On the principle of impedance-matching for underactuated wave energy harvesting systems. *Applied Ocean Research*, 118, 102958.

Faedo, N., García-Violini, D., Peña-Sanchez, Y., and Ringwood, J.V. (2020). Optimisation-vs. non-optimisation-based energy-maximising control for wave energy converters: A case study. In *European Control Conference (ECC)*, 843–848. IEEE.

Fuhrmann, P. (1989). Elements of factorization theory from a polynomial point of view. In *Three decades of mathematical system theory*, 148–178. Springer.

Fusco, F. and Ringwood, J.V. (2012). A simple and effective real-time controller for wave energy converters. *IEEE Transactions on sustainable energy*, 4(1), 21–30.

García-Violini, D., Faedo, N., Jaramillo-Lopez, F., and Ringwood, J.V. (2020). Simple controllers for wave energy devices compared. *Journal of Marine Science and Engineering*, 8(10), 793.

García-Violini, D., Peña-Sanchez, Y., Faedo, N., Windt, C., Ferri, F., and Ringwood, J.V. (2021). Experimental implementation and validation of a broadband lti energy-maximizing control strategy for the wavestar device. *IEEE Transactions on Control Systems Technology*, 29(6), 2609–2621.

Korde, U.A. and Ringwood, J.V. (2016). *Hydrodynamic control of wave energy devices*. Cambridge University Press.

Ljung, L. (1999). *System Identification: Theory for the User*. Prentice Hall information and system sciences series. Prentice Hall PTR.

Ochi, M.K. (1998). *Ocean Waves: The Stochastic Approach*. Cambridge Ocean Technology Series. Cambridge University Press.

Ringwood, J.V. (2020). Wave energy control: status and perspectives 2020. *IFAC-PapersOnLine*, 53(2), 12271–12282.

Thomas, R.L. (1976). *A practical introduction to impedance matching*. Artech House on Demand.